A Three-Phase Isolated Bidirectional AC/DC Converter and its Modified SVPWM Algorithm

Ling Gu, *Student Member, IEEE*, and Ke Jin, *Member, IEEE*

***Abstract*—This paper proposes a three-phase isolated bidirectional ac/dc converter. The converter achieves buck–boost ac/dc bidirectional conversion, sinusoidal ac current, and high-frequency electrical isolation with single-stage structure. The traditional SVPWM algorithm should be modified to keep the voltage–second balance of the transformer. The circuit derivation, operation principles, and SVPWM algorithm are presented specifically. The solution for shoot-through problem is proposed, which does not need extra dead time. To verify the theoretical analysis, the proposed converter was simulated by MATLAB/SIMULINK and a 3 kW prototype was built in the lab. The simulation and experimental results show the high power factor and the low harmonic distortion characteristics of the circuit.**

***Index Terms*—Bidirectional ac/dc converter, dc microgrid, SVPWM, three-phase inverter.**

I. Introduction

With the increasingly serve energy crisis and environmental pollution, the application of renewable energy, such as photovoltaic power generation, wind power generation, and tidal power generation, has attracted more and more attention [1], [2]. However, renewable energy is susceptible to the natural conditions and has unstable voltage and power. Hence, the renewable energy is always connected to the grid to constitute the microgrid, which can effectively solve the power fluctuation of the system. The research for 380-V dc microgrid has been popular with many experts around the world as it presents better efficiency and reliability with fewer power stages [3]–[5]. In high power applications, three-phase bidirectional ac/dc converter is always needed as grid-interface converter to achieve bidirectional energy flow between the grid and dc bus [6]–[11].

The common solution for grid-interface converter is three-phase voltage-source PWM rectifier [12]–[14], which generally converts three-phase 380-V ac voltage to 600–800-V dc voltage and does not achieve electrical isolation. Accordingly, it is necessary that a dc/dc converter and a three-phase PWM converter constitute a two-stage structure [15] or utilize a power frequency transformer in the grid-interface converter application, which increases the volume and reduces the efficiency.

Three-phase current-source PWM rectifier can achieve ac/dc buck conversion with single-stage structure [16]. But its input current is discontinuous and has low power factor. Furthermore, it still does not achieve electrical isolation. Another available solution is three-phase isolated ac/dc converter, such as VIENNA rectifier II [17]. It has continuous sinusoidal behavior of the input current and high-frequency isolation with single-stage structure. However, its bidirectional switch consists of four diodes and one active switch, which brings large conduction loss in high power application. And it is a unidirectional converter and cannot transfer energy from dc side to ac side.

An isolated three-phase soft-switched buck rectifier is proposed by Vlatkovic *et al.* [18]. By using an auxiliary circuit with a simple method of energy recovery, the current is diverted away from the main power switches before they are turned OFF. And the switching power loss of the converter is decreased by using zero-current switching method. A three-phase buck rectifier with high-frequency isolation by single stage is introduced in [19]. The topology utilizes a forward/flyback transformer to allow the high-frequency isolation. But the two converters have common disadvantages with large conduction loss and low input power factor. Furthermore, neither the forward converter nor the forward-flyback converter is suitable for high power application. Conergy neutral point-clamped (NPC) topology is suitable for PV power generation application as its low conduction loss [20]. It achieves bidirectional power flow between ac and dc side. But it does not achieve electrical isolation and cannot convert three-phase 380-V ac voltage to 380-V dc voltage directly with single-stage structure.

To achieve buck–boost ac/dc conversion and electrical isolation as well, this paper proposes a three-phase isolated bidirectional ac/dc converter, which is derived from the conergy NPC topology. Compared with two-stage solution, the converter removes decoupling capacitor and dc–dc converter's filter inductor, and no extra dead time is needed to avoid the shoot-through problem. The PI control system based on the modified SVPWM algorithm is built. The operation principles are presented and the shoot-through problem is analyzed specifically. A 3 kW prototype with the controller TMS320F2812 was built in the lab and the experimental results verify the theoretical analysis well.

Manuscript received August 18, 2014; revised October 21, 2014; accepted November 24, 2014. Date of publication December 5, 2014; date of current version May 22, 2015. This work was supported in part by the National Natural Science Foundation of China under Grant 51377080, by the Fok Ying Tong Education Foundation under Grant 131056, by the Natural Science Foundation for Distinguished Young Scholars of Jiangsu Province (BK20130036), by the Industry-Academia Cooperation Innovation Fund of Jiangsu Province-Prospective Joint Research Project(BY2012016), by the Lite-On Power Electronics Technology Research Fund, by the Jiangsu Key Laboratory of New Energy Generation and Power Conversion Open Research Fund, and by the Nanjing University of Aeronautics and Astronautics Fundamental Research Funds under Grant NE2013102. Recommended for publication by Associate Editor A. M. Trzynadlowski.

The authors are with the Jiangsu Key-Laboratory of New Energy Generation and Power Conversion, College of Automation Engineering, Nanjing University of Aeronautics and Astronautics, Nanjing 210016, China (e-mail: guling@nuaa.edu.cn; jinke@nuaa.edu.cn).

Color versions of one or more of the figures in this paper are available online at http://ieeexplore.ieee.org.

Digital Object Identifier 10.1109/TPEL.2014.2378274

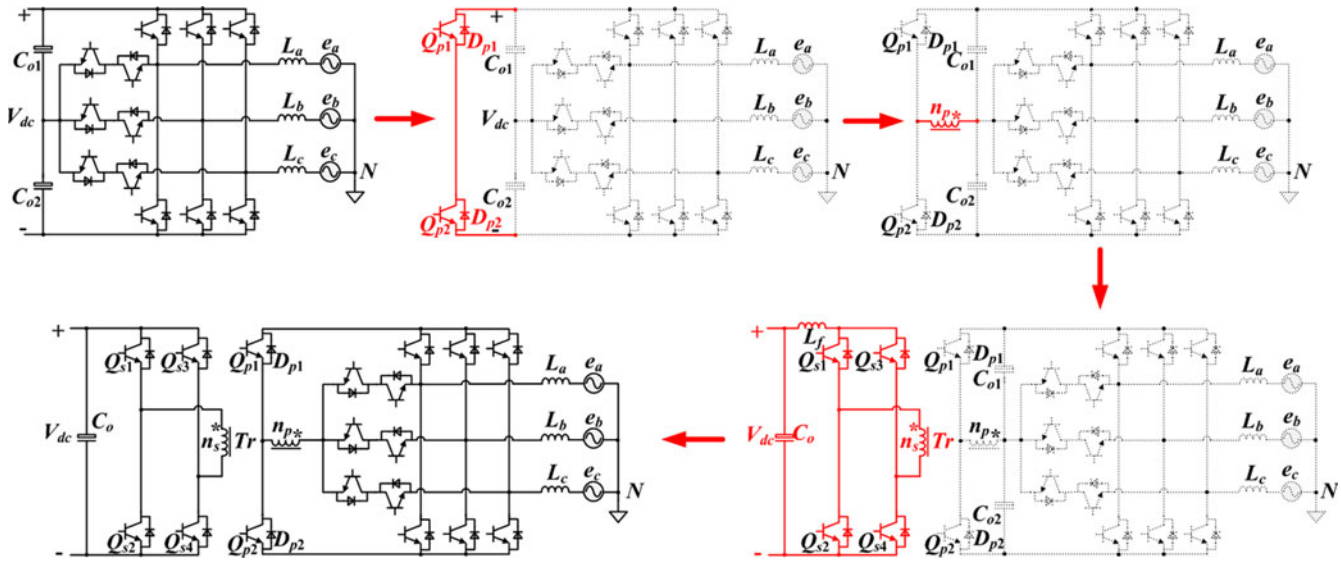

Fig. 1. Circuit derivation.

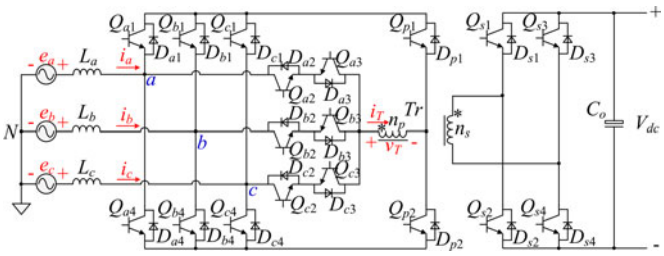

Fig. 2. Main circuit.

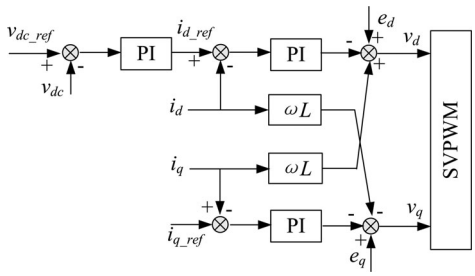

Fig. 3. PI control system.

II. Circuit Derivation and Control Strategy

A. Circuit Derivation

The proposed three-phase bidirectional ac/dc converter is derived from the conergy NPC topology. The specific derivation procedure is as follows (see Fig. 1):

1) add a bridge composed of two active switches Q_{p1} and Q_{p2};
2) add a transformer whose primary side is connected to the neutral point of the added bridge and the junction of two capacitors C_{o1} and C_{o2};
3) add two bridges composed of four active switches Q_{s1}, Q_{s2}, Q_{s3}, Q_{s4}, and a filter inductor L_f at the secondary side of the transformer, a two-stage bidirectional ac/dc converter is derived;
4) remove C_{o1}, C_{o2}, and L_f. Then, a single-stage bidirectional ac/dc converter shown by Fig. 2 is derived.

B. Control Strategy

Fig. 3 shows the control system. With the voltage and current dual-loop control system, the current controller is designed in *dq* rotary two-phase coordinates to maintain the adjustable dc voltage and ac current with unity power factor.

TABLE I
Conducting Components

	Rectifier Mode	Inverter Mode
Active Switches	$Q_{i2}, Q_{i3}, Q_{p1}, Q_{p2}$ $(i = a, b, c)$	$Q_{i1}, Q_{i2}, Q_{i3}, Q_{i4}$, $Q_{s1}, Q_{s2}, Q_{s3}, Q_{s4}$,
Diodes	$D_{i1}, D_{i2}, D_{i3}, D_{i4}$, $D_{s1}, D_{s2}, D_{s3}, D_{s4}$	$D_{p1}, D_{p2}, D_{i2}, D_{i3}$,

Through analysis, the SVPWM algorithm for nonisolated converter [21]–[23] is not suitable for the proposed converter, since the control strategy for the proposed converter should take both the voltage–second balance of the transformer and the current direction's influence on the voltage vectors into considerations.

III. Operation Principles

A. Conducting Components

Due to different current direction under rectifier mode and inverter mode, the conducting switches are also different, which is shown by Table I.

TABLE II
SWITCHING STATES DEFINITION

S_i	Q_{i1}	Q_{i2}	Q_{i3}	Q_{i4}	$S_d S_e$	Q_{p1}	Q_{p2}	$Q_{s1,4}$	$Q_{s2,3}$
0^+	ON	OFF	OFF	OFF	10	ON	OFF	OFF	OFF
1^-	OFF	ON	OFF	OFF	01	OFF	ON	OFF	OFF
1^+	OFF	OFF	ON	OFF	11	ON	ON	OFF	OFF
0^-	OFF	OFF	OFF	ON	10	OFF	OFF	ON	OFF
1	OFF	ON	ON	OFF	01	OFF	OFF	OFF	ON
0	OFF	OFF	OFF	OFF	00	OFF	OFF	OFF	OFF

B. Switching States Definition

The switching states are defined by $j = (S_a S_b S_c)^{\mathrm{sign}\{v_T\}}_{S_d S_e}$. $S_a, S_b, S_c (S_i, i = a, b, c)$ represents the switching states of the switches Q_{a1-4}, Q_{b1-4}, and Q_{c1-4}. S_d and S_e represent the switching states of the switches Q_{p1} and Q_{p2} under rectifier mode and $Q_{s\,1,\,4}$ and $Q_{s\,2,\,3}$ under inverter mode. Sign $\{v_T\}$ represents the voltage direction of the transformer. The specific definition is shown by Table II.

C. Operation Modes

Before analysis, the following assumptions are made:1) All the components are ideal. 2) The three-phase current is sinusoidal and in phase with the three-phase voltage under rectifier mode and in opposite phase with the voltage under inverter mode. 3) The capacitor C_o is large enough to be treated as a voltage source.

All the reference direction of voltage and current is shown in Fig. 2. As the symmetry of three-phase current, the operation modes when $e_a > 0$, $e_b < 0$, and $e_c < 0$ are selected for example to do specific analysis.

1) Inverter Mode ($i_a < 0$, $i_b > 0$, $i_c > 0$): Mode 1 [$j = (0^+1^-1^-)^-_{01}$, Fig. 4(a)]: The switches Q_{s2}, Q_{s3}, Q_{a1}, Q_{b2}, and Q_{c2} are turned ON, and the diodes D_{p1}, D_{b3}, and D_{c3} conduct. The primary current flows into the homonymous end of the transformer and the voltage across the transformer is negative. Energy flows from dc side to ac side.

Mode 2 [$j = (1^+0^-0^-)^+_{10}$, Fig. 4(b)]: The switches Q_{s1}, Q_{s4}, Q_{a3}, Q_{b4}, and Q_{c4} are turned ON, and the diodes D_{p2} and D_{a2} conduct. The primary current flows out of the homonymous end of the transformer and the voltage across the transformer is positive. Energy flows from dc side to ac side.

Mode 3 [$j = (1^+0^-1^-)^+_{10}$, Fig. 4(c)]: The switches Q_{s1}, Q_{s4}, Q_{a3}, Q_{b4}, and Q_{c2} are turned ON, and the diodes D_{p2}, D_{a2}, and D_{c3} conduct. The primary current flows out of the homonymous end of the transformer and the voltage across the transformer is positive. Energy flows from dc side to ac side.

Mode 4 [$j = (1^+1^-0^-)^+_{10}$, Fig. 4(d)]: The switches Q_{s1}, Q_{s4}, Q_{a3}, Q_{b2}, and Q_{c4} are turned ON, and the diodes D_{p2}, D_{a2}, and D_{b3} conduct. The primary current flows out of the homonymous end of the transformer and the voltage across the transformer is positive. Energy flows from dc side to ac side.

Mode 5 [$j = (1^+1^-1^-)^0_{00}$, Fig. 4(e)]: The switches Q_{a3}, Q_{b2}, and Q_{c2} are turned ON, and the diodes D_{a2}, D_{b3}, and D_{c3} conduct. The voltage across the transformer is zero, and there is no energy flowing from dc side to ac side. It is called zero state. The switching states $j = (0^+0^-0^-)^0_{00}$, $j = (0^+0^-1^-)^0_{00}$, and $j = (0^+1^-0^-)^0_{00}$ are also zero states.

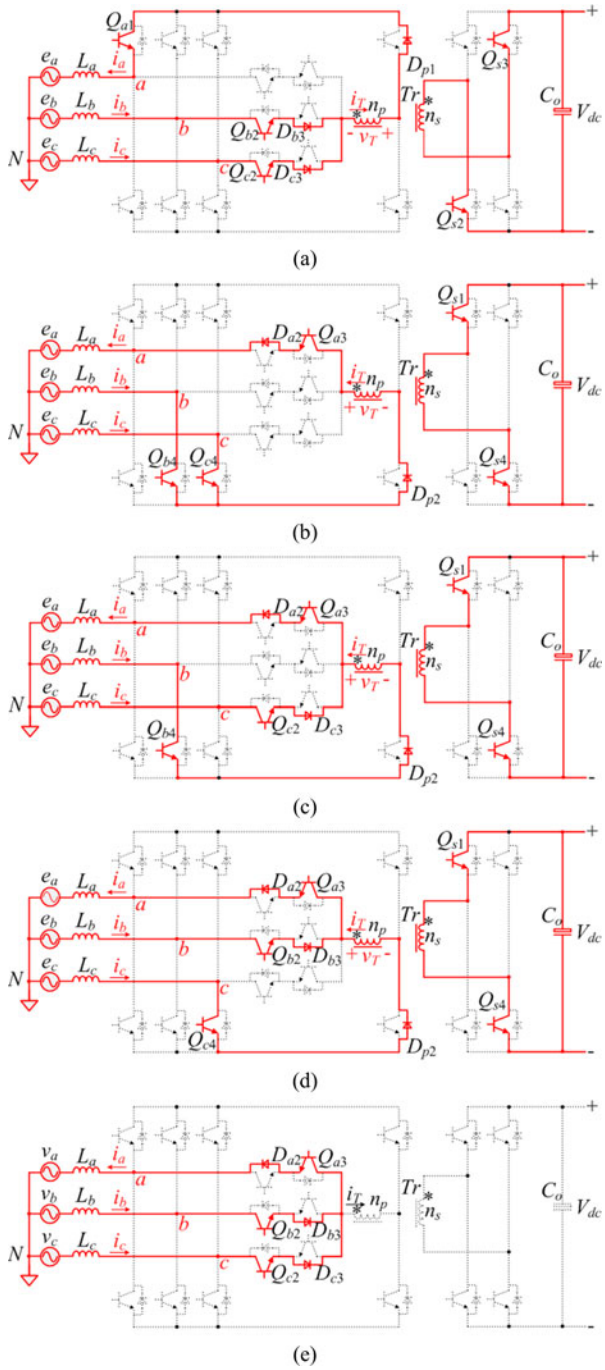

Fig. 4. Operation modes under inverter mode.

2) Rectifier Mode ($i_a > 0$, $i_b < 0$, $i_c < 0$): Mode 1 [$j = (01^+1^+)^-_{10}$, Fig. 5(a)]: The switches Q_{b3}, Q_{c3}, and Q_{p1} are turned ON, and the diodes D_{a1}, D_{b2}, D_{c2}, D_{s2}, and D_{s3} conduct. The primary current flows out of the homonymous end of the transformer and the voltage across the transformer is negative. Energy flows from ac side to dc side.

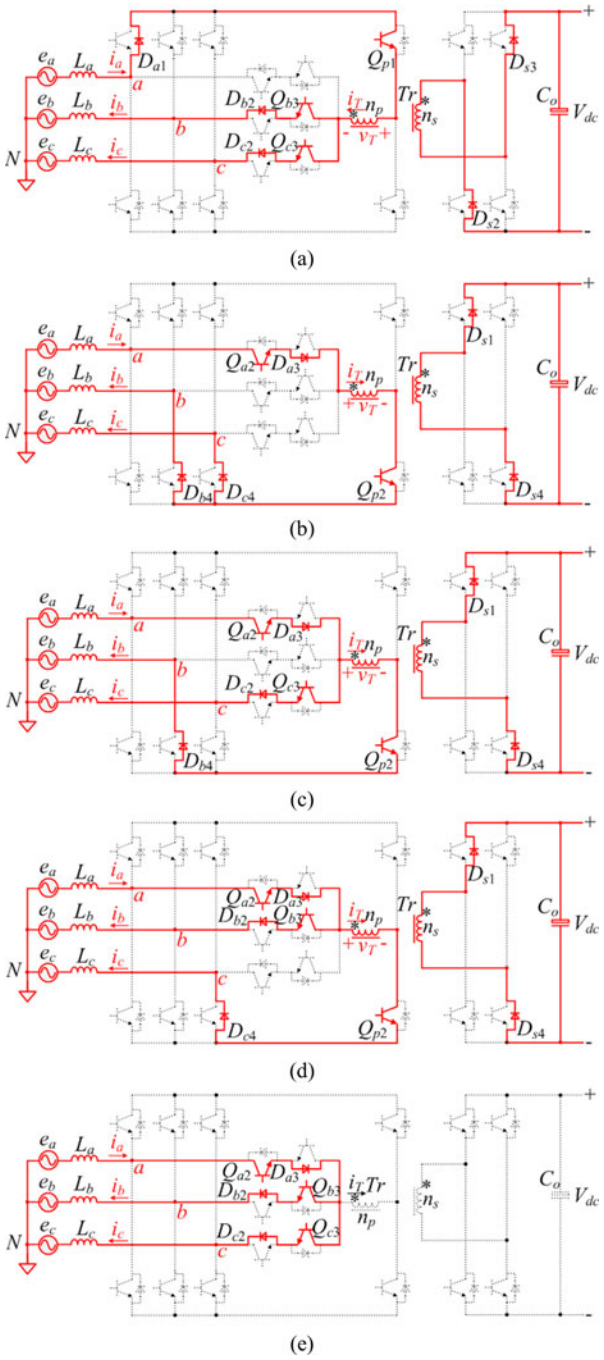

Fig. 5. Operation modes under rectifier mode.

Mode 2 [$j = (1^{-}00)^{+}_{01}$, Fig. 5(b)]: The switches Q_{a2} and Q_{p2} are turned ON, and the diodes D_{a3}, D_{b4}, D_{c4}, D_{s1}, and D_{s4} conduct. The primary current flows into the homonymous end of the transformer and the voltage across the transformer is positive. Energy flows from ac side to dc side.

Mode 3 [$j = (1^{-}01^{+})^{+}_{01}$, Fig. 5(c)]: The switches Q_{a2}, Q_{c3}, and Q_{p2} are turned ON, and the diodes D_{a3}, D_{b4}, D_{c2}, D_{s1}, and D_{s4} conduct. The primary current flows into the homonymous end of the transformer and the voltage across the transformer is positive. Energy flows from ac side to dc side.

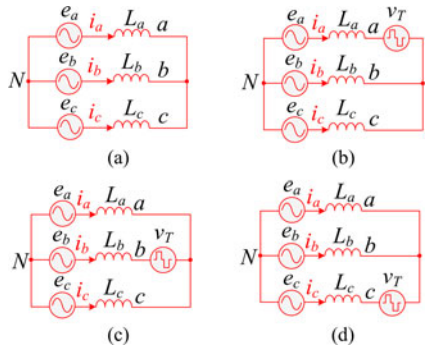

Fig. 6. Equivalent circuits.

Mode 4 [$j = (1^{-}1^{+}0)^{+}_{01}$, Fig. 5(d)]: The switches Q_{a2}, Q_{b3}, and Q_{p2} are turned ON, and the diodes D_{a3}, D_{b2}, D_{c4}, D_{s1}, and D_{s4} conduct. The primary current flows into the homonymous end of the transformer and the voltage across the transformer is positive. Energy flows from ac side to dc side.

Mode 5 [$j = (1^{-}1^{+}1^{+})^{0}_{11}$, Fig. 5(e)]: The switches Q_{a2}, Q_{b3}, Q_{c3}, Q_{p1}, and Q_{p2} are turned ON, and the diodes D_{a3}, D_{b2}, and D_{c2} conduct. It is zero state. The switching states $j = (000)^{0}_{11}$, $j = (001^{+})^{0}_{11}$, and $j = (01^{+}0)^{0}_{11}$ are also zero states.

D. Equivalent Circuits

Through analysis, the proposed converter has altogether four equivalent circuits in spite of various switching states under inverter or rectifier mode, which is shown by Fig. 6. v_T is the voltage across the transformer, which is regarded as a current-controlled voltage source and whose value depends on the current direction of the transformer. So circuit (b), (c), and (d) each have two conditions $v_T = (n_p/n_s)V_{\rm dc}$ and $v_T = -(n_p/n_s)V_{\rm dc}$. The voltage vector is defined as follows:

$$\boldsymbol{v} = v_{aN} + \boldsymbol{\alpha} v_{bN} + \boldsymbol{\alpha}^2 v_{cN} \tag{1}$$

where $\boldsymbol{\alpha} = e^{j\frac{2}{3}\pi}$. The circuit (a) forms zero vectors and circuit (b), (c), and (d) forms six nonzero vectors.

IV. SVPWM Algorithm

A. Sector Partition

The relationship between the voltage vectors $\boldsymbol{v}$ and switching states is shown in Table III by taking the rectifier mode when $i_a > 0, i_b < 0, i_c < 0$, and $i_a > 0, i_b > 0, i_c < 0$ for example.

Through the above analysis, there are altogether six basic nonzero vectors, which divide the whole cycle into six sectors. From Table III, it is concluded that the voltage vectors formed by the switch states are also influenced by the direction of current flowing in the transformer, so the sector partition should take both the basic vectors and current direction of i_a, i_b, and i_c into considerations, which is shown by Fig. 7. The full lines divide the cycle into six sectors according to the basic voltage vectors as the traditional partition. The dotted lines further divide it into 12 sectors according to the three-phase ac current direction. To distinguish the 12 sectors, sectors are numbered according to

TABLE III
VOLTAGE VECTORS VERSUS SWITCHING STATES

$i_a>0, i_b<0, i_c<0$							$i_a>0, i_b>0, i_c<0$						
S_a	S_b	S_c	S_d	S_e	Sign $\{v_T\}$	$\boldsymbol{v}$	S_a	S_b	S_c	S_d	S_e	Sign $\{v_T\}$	$\boldsymbol{v}$
0	0	0	1	1	0	0	0	0	0	1	1	0	0
0	0	1^+	1	1	0	0	0	0	1^+	1	0	-	$-\alpha^2(2n_p/3n_s)V_{\rm dc}$
0	1^+	0	1	1	0	0	0	1^-	0	1	1	0	0
0	1^+	1^+	1	0	-	$(2n_p/3n_s)V_{\rm dc}$	0	1^-	1^+	1	0	-	$(2n_p/3n_s)V_{\rm dc}$
1^-	0	0	0	1	+	$(2n_p/3n_s)V_{\rm dc}$	1^-	0	0	1	1	0	0
1^-	0	1^+	0	1	+	$-\alpha(2n_p/3n_s)V_{\rm dc}$	1^-	0	1^+	1	0	-	$\alpha(2n_p/3n_s)V_{\rm dc}$
1^-	1^+	0	0	1	+	$-\alpha^2(2n_p/3n_s)V_{\rm dc}$	1^-	1^-	0	0	1	+	$-\alpha^2(2n_p/3n_s)V_{\rm dc}$
1^-	1^+	1^+	1	1	0	0	1^-	1^-	1^+	1	1	0	0

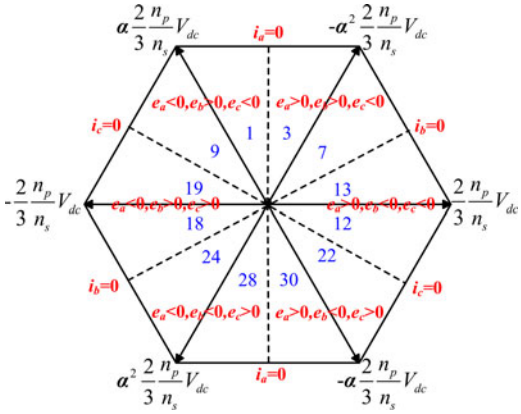

Fig. 7. Sector Partition.

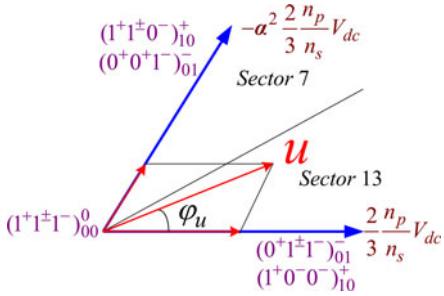

Fig. 8. Sectors 13 and 7 under inverter mode.

the value of three-phase voltage v_α and v_β in stationary two-phase coordinates. Therefore, set six intermediate variables as follows:

$$v_{\rm ref1} = v_\beta \tag{2}$$

$$v_{\rm ref2} = v_\alpha \tag{3}$$

$$v_{\rm ref3} = \frac{1}{2}(\sqrt{3}v_\alpha - v_\beta) \tag{4}$$

$$v_{\rm ref4} = \frac{1}{2}(v_\alpha - \sqrt{3}v_\beta) \tag{5}$$

$$v_{\rm ref5} = \frac{1}{2}(-\sqrt{3}v_\alpha - v_\beta) \tag{6}$$

$$v_{\rm ref6} = \frac{1}{2}(-v_\alpha - \sqrt{3}v_\beta). \tag{7}$$

If $v_{\rm ref1}>0$, $A=1$; otherwise, $A=0$. If $v_{\rm ref2}>0$, $B=1$; otherwise, $B=0$. If $v_{\rm ref3}>0$, $C=1$; otherwise, $C=0$. If $v_{\rm ref4}>0$, $D=1$; otherwise, $D=0$. If $v_{\rm ref5}>0$, $E=1$; otherwise, $E=0$. If $v_{\rm ref6}>0$, $F=1$; otherwise, $F=0$. The sector number is defined by $N=A+2B+4C+6D+8E+10F$. The numbers of each sector are shown by Fig. 7.

B. Vector Synthesis Method

For vector synthesis, it should obey the following laws: 1) keep the voltage–second balance of the transformer; 2) reduce the switching loss; and 3) reduce the conduction loss.

Take the sectors 13 and 7 (see Fig. 8) for example to introduce the specific vector synthesis method.

1) Inverter Mode: In sector $13(i_a<0, i_b>0, i_c>0)$, two nonzero vectors in two directions are enough to form the target vector as traditional SVPWM algorithm for three-phase full-bridge inverter. But they cannot guarantee the voltage–second balance of the transformer. So three nonzero vectors should be selected and the switching-state sequence is as follows:

$$\begin{aligned}(1^+0^-0^-)^+_{10} &\rightarrow (1^+1^-0^-)^+_{10} \rightarrow (1^+1^-1^-)^0_{00}\\ \rightarrow (0^+1^-1^-)^-_{01}|_{t=T_s/2} &\rightarrow (0^+1^-1^-)^-_{01} \rightarrow (1^+1^-1^-)^0_{00}\\ \rightarrow (1^+1^-0^-)^+_{10} &\rightarrow (1^+0^-0^-)^+_{10}|_{t=T_s}.\end{aligned} \tag{8}$$

In sector $7(i_a<0, i_b<0, i_c>0)$, the switching-state sequence is as follows:

$$\begin{aligned}(0^+0^+1^-)^-_{01} &\rightarrow (0^+1^+1^-)^-_{01} \rightarrow (1^+1^+1^-)^0_{00}\\ \rightarrow (1^+1^+0^-)^+_{10}|_{t=T_s/2} &\rightarrow (1^+1^+0^-)^+_{10} \rightarrow (1^+1^+1^-)^0_{00}\\ \rightarrow (0^+1^+1^-)^-_{01} &\rightarrow (0^+0^+1^-)^-_{01}|_{t=T_s}.\end{aligned} \tag{9}$$

The driving signals in sectors 13 and 7 under inverter mode are shown by Fig. 9.

2) Rectifier Mode: In sector $13(i_a>0, i_b<0, i_c<0)$, the switching-state sequence is as follows:

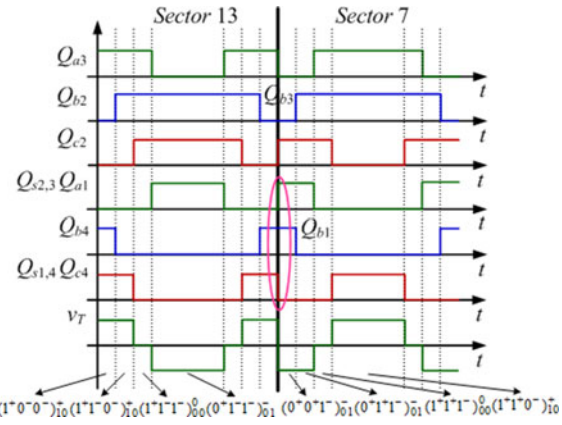

Fig. 9. Driving signals in sectors 13 and 7 under inverter mode.

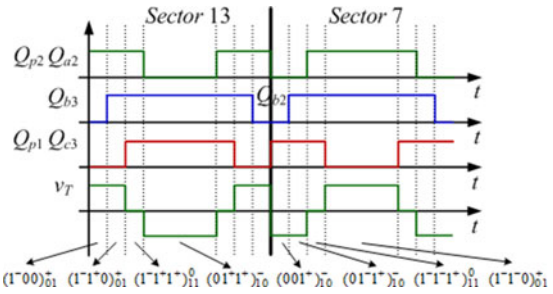

Fig. 10. Driving signals in sectors 13 and 7 under rectifier mode.

$$\begin{aligned}(1^-00)^+_{01} &\rightarrow (1^-1^+0)^+_{01} \rightarrow (1^-1^+1^+)^0_{11}\\ \rightarrow (01^+1^+)^-_{10}|_{t=T_s/2} &\rightarrow (01^+1^+)^-_{10} \rightarrow (1^-1^+1^+)^0_{11}\\ \rightarrow (1^-1^+0)^+_{01} &\rightarrow (1^-00)^+_{01}|_{t=T_s}. \end{aligned} \tag{10}$$

In sector 7($i_a > 0, i_b > 0, i_c < 0$), the switching-state sequence is as follows:

$$\begin{aligned}(001^+)^-_{10} &\rightarrow (01^-1^+)^-_{10} \rightarrow (1^-1^-1^+)^0_{11}\\ \rightarrow (1^-1^-0)^+_{01}|_{t=T_s/2} &\rightarrow (1^-1^-0)^+_{01} \rightarrow (1^-1^-1^+)^0_{11}\\ \rightarrow (01^-1^+)^-_{10} &\rightarrow (001^+)^-_{10}|_{t=T_s}. \end{aligned} \tag{11}$$

The driving signals in sectors 13 and 7 under rectifier mode are shown by Fig. 10.

C. Equivalent Modulation Waves

To calculate the duty cycle of each switching state, three intermediate variables are set

$$X = \frac{\sqrt{3}v_\beta}{(n_p/n_s)V_{\rm dc}} \tag{12}$$

$$Y = \frac{(\frac{\sqrt{3}}{2}v_\beta + \frac{3}{2}v_\alpha)}{(n_p/n_s)V_{\rm dc}} \tag{13}$$

$$Z = \frac{(\frac{\sqrt{3}}{2}v_\beta - \frac{3}{2}v_\alpha)}{(n_p/n_s)V_{\rm dc}}. \tag{14}$$

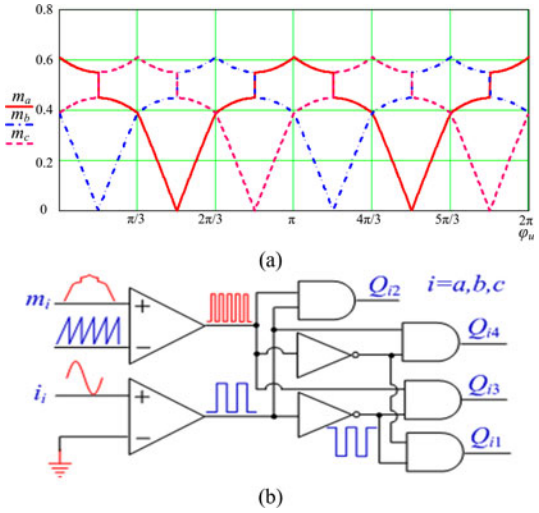

Fig. 11. Equivalent modulation waves and driving signals.

In sector 13 under inverter mode, the duty cycle should meet the following equations:

$$\delta_{(1^+0^-0^-)^+_{10}} + \delta_{(0^+1^-1^-)^-_{01}} = -Z \tag{15}$$

$$\delta_{(1^+1^-0^-)^+_{10}} = X \tag{16}$$

$$\delta_{(1^+0^-0^-)^+_{10}} + \delta_{(1^+1^-0^-)^+_{10}} = \delta_{(0^+1^-1^-)^-_{01}}. \tag{17}$$

Then, the duty cycle of each vector can be calculated. The three-phase equivalent modulation waves under inverter mode are shown by Fig. 11(a), which are the same as rectifier mode. The driving signals generation of the switches $Q_{i1-4}(i = a, b, c)$ based on the modulation waves is shown by Fig. 11(b).

V. Circuit Characteristics

A. Shoot-Through Problem Analysis of DC Side

When the converter operates under inverter mode, the shoot-through problem of dc side should be noticed. It is seen from Fig. 9 that the dead time between the driving signals of $Q_{s1,4}$ and $Q_{s2,3}$ is half of the zero vector time within each sector. Enough zero vector time can avoid the shoot-through problem. However, it is clear that at the junction of sectors 13 and 7, there is no dead time between the driving signals of $Q_{s1,4}$ and $Q_{s2,3}$, which may result the shoot-through of the dc side. If we change the switching sequence of sector 13 as (18), the problem will be solved as a half of the zero vector time of sector 13 serves as the dead time, which is shown by Fig. 12. The equivalent modulation waves in whole cycle are shown by Fig. 13

$$\begin{aligned}(0^+1^-1^-)^-_{01} &\rightarrow (1^+1^-1^-)^0_{00} \rightarrow (1^+1^-0^-)^+_{10}\\ \rightarrow (1^+0^-0^-)^+_{10}|_{t=T_s/2} &\rightarrow (1^+0^-0^-)^+_{10} \rightarrow (1^+1^-0^-)^+_{10}\\ \rightarrow (1^+1^-1^-)^0_{00} &\rightarrow (0^+1^-1^-)^-_{01}|_{t=T_s}. \end{aligned} \tag{18}$$

Similarly, the switching sequence in sector 13 remains unchanged, and the switching sequence in sector 7 is changed

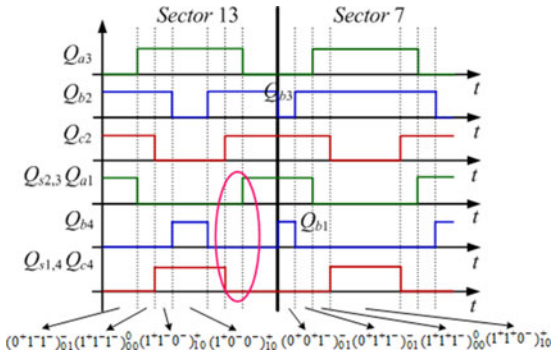

Fig. 12. Driving signals in sectors 13 and 7 with sector 13 changed.

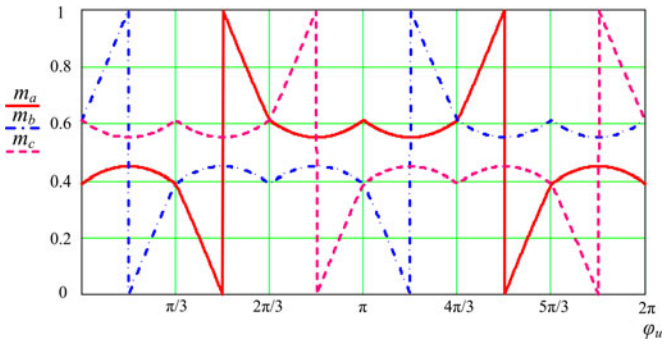

Fig. 13. Equivalent modulation waves with sector 13 changed.

as follows:

$$(1^+1^+0^-)^+_{10} \rightarrow (1^+1^+1^-)^0_{00} \rightarrow (0^+1^+1^-)^-_{01} \rightarrow (0^+0^+1^-)^-_{01}|_{t=T_s/2} \rightarrow (0^+0^+1^-)^-_{01}| \rightarrow (0^+1^+1^-)^-_{01} \rightarrow (1^+1^+1^-)^0_{00} \rightarrow (1^+1^+0^-)^+_{10}|_{t=T_s}. \quad (19)$$

In this case, a half of the zero vector time of sector 7 serves as the dead time. It is concluded that the shoot-through problem resulted by the dc-side's switches can be solved by adjusting the switching sequence.

B. Control of Bidirectional Switches

Under rectifier mode, the bidirectional switches Q_{i2} and Q_{i3} can be turned ON synchronously for simplification. However, under inverter mode, the shoot-through problem may occur when Q_{i2} and Q_{i3} are turned ON synchronously and there is no dead time between the driving signals of $Q_{i2,3}$ and $Q_{i1,4}$. Taking sector 13 for example, from $(1^+0^-0^-)^+_{10}$ to $(1^+1^-0^-)^+_{10}$, both Q_{b3} and Q_{b4} may be ON and the shoot-through problem may occur, which is shown by Fig. 14(a).

To avoid this situation, the driving signals of Q_{b2} and Q_{b3} should be separate. Then, even if Q_{b2} and Q_{b4} are turned ON synchronously, there will not exist any shoot-through problem as D_{p2} and D_{b3} block both forward and reverse current, which is shown by Fig. 14(b).

In a word, the proposed converter does not have any shoot-through problem with proper control strategy and need not extra dead time.

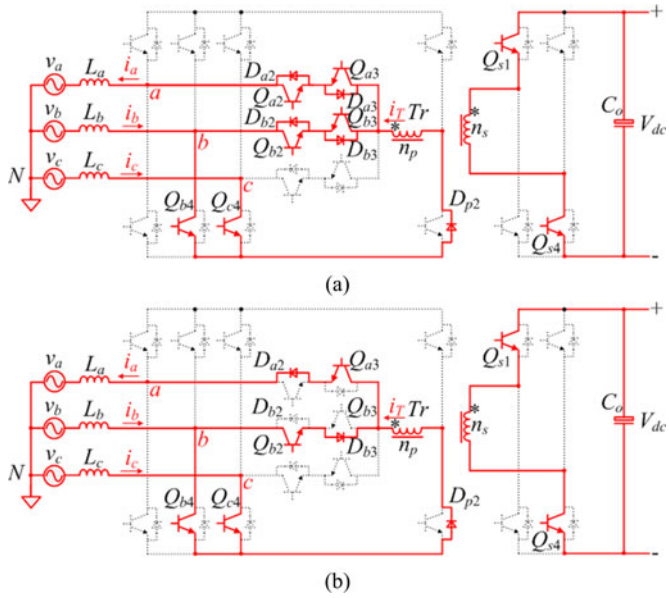

Fig. 14. Shoot-through mode of the converter.

C. Comparison With Some Other Converters

The single-stage boost-derived matrix PWM rectifier has the similar topology and function as the proposed converter. Compared with matrix rectifier ([24], Fig. 9), the proposed converter has two more switches. However, for the proposed converter, only eight switches need to be controlled under rectifier mode, and 16 switches need to be controlled under inverter mode; while 12 switches need to be controlled under rectifier mode, and 16 switches need to be controlled under inverter mode for matrix converter. Under rectifier mode, the proposed converter's switches $Q_{i2,3}(i = a, b, c)$ can also be turned ON synchronously, so it is clear that the control is simpler than the matrix one. What's more, for the proposed converter and SVPWM algorithm, the time of zero vectors can serve as the dead time, which avoid the shoot-through problem naturally, while the matrix converter needs extra dead time.

The traditional three-phase Z-source inverter [25] is popular as it achieves both step-up and step-down output and solves the shoot-through problem. Comparing the proposed converter and Z-source inverter, although the proposed converter has more switches, it still has following advantages: 1) Fewer capacitors and magnetic components. 2) Achievement of both bidirectional power flow and high-frequency isolation. The Z-source network always needs the capacitors with large capacitance and high voltage stress and the inductors with large inductance, which increases the volume and weight, and it cannot be applied as grid-interface inverter directly without electrical isolation. Jiang *et al.* [26] proposes a high frequency transformer isolated Z-source inverter. However, its Z-source network needs two transformers and four capacitors, which decreases the power density.

D. Power Loss Analysis

The power loss analysis of the proposed converter under rectifier mode is as follows:

The conduction loss, switching loss, and reverse recovery loss of bidirectional switches $Q_{a2,3}$, $Q_{b2,3}$, and $Q_{c2,3}$ is

$$P_{bi\_\mathrm{cond}} = 3I_{bi\_\mathrm{avg}} \cdot (V_{ce} + V_d) = 11.66\ \mathrm{W} \quad (20)$$

$$P_{bi\_\mathrm{sw}} = 3f_s \cdot (E_{\mathrm{on}} + E_{\mathrm{off}}) = 35.34\ \mathrm{W} \quad (21)$$

$$P_{bi\_rr} = 6 \times \frac{1}{4} \times \left(\frac{n_p}{n_s} V_{\mathrm{dc}}\right) I_{rr} t_{rr} \frac{f_s}{2} = 1.72\ \mathrm{W}. \quad (22)$$

The driving loss is so small compared to other loss that it can be neglected.

The conduction loss of the three-phase bridge $D_{a1,4}$, $D_{b1,4}$, and $D_{c1,4}$ is

$$P_{th\_\mathrm{cond}} = 6I_{th\_\mathrm{avg}} \cdot V_d = 5.51\ \mathrm{W} \quad (23)$$

$$P_{th\_rr} = 6 \times \frac{1}{4} \times \left(\frac{n_p}{n_s} V_{\mathrm{dc}}\right) I_{rr} t_{rr} \frac{f_s}{2} = 1.72\,\mathrm{W}. \quad (24)$$

The conduction loss and switching loss of $Q_{p1,2}$ is

$$P_{p\_\mathrm{cond}} = 2I_{p\_\mathrm{avg}} \cdot V_{ce} = 5.32\ \mathrm{W} \quad (25)$$

$$P_{p\_\mathrm{sw}} = 2f_s \cdot (E_{\mathrm{on}} + E_{\mathrm{off}}) = 30.64\ \mathrm{W}. \quad (26)$$

The conduction loss and reverse recovery loss of D_{s1-4} is

$$P_{d\_\mathrm{cond}} = 4I_{d\_\mathrm{avg}} \cdot V_d = 14.22\ \mathrm{W} \quad (27)$$

$$P_{d\_rr} = 4 \times \frac{1}{4} V_{\mathrm{dc}} I_{rr} t_{rr} f_s = 5.68\ \mathrm{W}. \quad (28)$$

For the inductors, the maximum flux density B_{pk} is

$$B_{pk} = \frac{V_{\mathrm{rms}}}{4.44 f_s A_e N} = 0.05\ T. \quad (29)$$

According to the core loss curves, the core loss is 20 mW/cm^3, so the power loss of the inductors is

$$P_L = 3(P_{L\_fe} + P_{L\_cu}) = 3(P_{L\_\mathrm{core}} V_{L\_e} + I^2_{L\_\mathrm{rms}} R_f) = 14.97\ \mathrm{W}. \quad (30)$$

For the transformer, the maximum flux density B_m is calculated as 0.138 T. The core loss is 10 mW/cm^3, and the power loss of the transformer is

$$P_{Tr} = P_{Tr\_fe} + P_{Tr\_cu} = P_{Tr\_\mathrm{core}} V_{Tr\_e} + (I^2_{Trp\_\mathrm{rms}} R_{Trp} + I^2_{Trs\_\mathrm{rms}} R_{Trs}) = 9.99\ \mathrm{W}. \quad (31)$$

Three-phase PWM rectifier [13] and VIENNA rectifier [27] are two common converters to achieve ac/dc conversion. However, they cannot achieve electrical isolation and buck–boost conversion. So a ZVS full-bridge (ZVS-FB) bidirectional dc/dc converter [28] is always added as the second stage. The loss comparison among the proposed converter, the two-stage converter with VIENNA rectifier and ZVS-FB, and the two-stage converter with three-phase PWM and ZVS-FB is shown by Fig. 15 when the total power is 3 kW under rectifier mode.

It is seen that VIENNA + ZVS-FB has the minimum conduction loss. However, according to the comparison shown by Table IV, it has more components than the proposed converter,

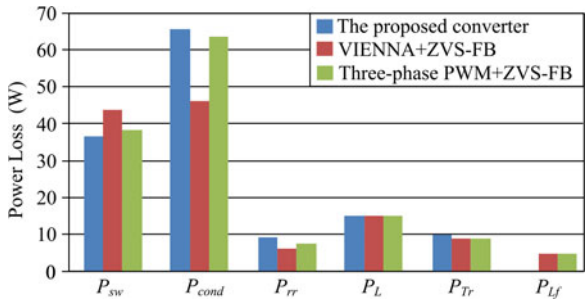

Fig. 15. Loss comparison with traditional converters.

TABLE IV
COMPONENTS COMPARISON

	The proposed converter	VIENNA + ZVS-FB	Three-phase PWM + ZVS-FB
Switches	18	20	14
Capacitors	Decoupling capacitors between two stages; Filter capacitors of dc side	Decoupling capacitors between two stages; Filter capacitors of dc side	Decoupling capacitors between two stages; Filter capacitors of dc side
Inductors	Filter inductors of ac side	Filter inductors of ac side and dc side	Filter inductors of ac side and dc side
Transformers	1	1	1

such as two active switches, decoupling capacitors between two stages, and filter inductor of dc side. It is seen that the power loss of the proposed converter and three-phase PWM + ZVS FB is close, but the proposed converter removes the decoupling capacitors and filter inductor of dc side. Besides, the proposed converter has no shoot-through problem without extra dead time.

Through the above comparison and power loss analysis, it is concluded that the converter has higher power density with fewer inductors and capacitors, and higher reliability without shoot-through problem. Furthermore, the decoupling capacitors with large capacitance between two stages always utilize electrolytic capacitors whose life influences the reliability of the converter, and the proposed converter's elimination of the decoupling capacitors will further improve the reliability.

E. Design Considerations of the Transformer

According to Figs. 7 and 8, the ac-phase voltage's peak value should meet the following equation:

$$v_{ap} \le \frac{\sqrt{3}}{3} \frac{n_p}{n_s} V_{\mathrm{dc}}. \quad (32)$$

Then for the given ac voltage and dc voltage, the turn ratio of the transformer can be calculated.

According to (32), turn ratio is selected to be 2/3. EE85B is chosen as the transformer magnetic core and its effective cross-sectional area A_e is 859 mm^2, and the maximum flux density B_m should meet the following equation:

$$B_m = \frac{V_{\mathrm{dc}}}{4 f_s A_e n_s} < 0.16\ \mathrm{T}. \quad (33)$$

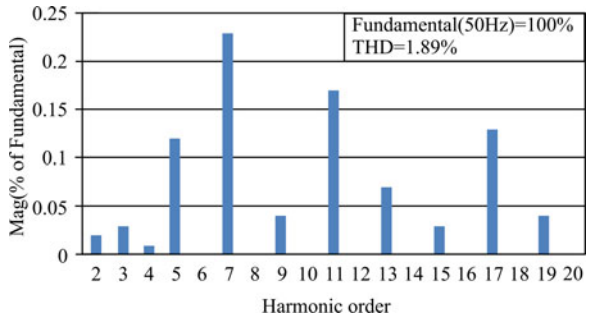

Fig. 16. Simulation results under rectifier mode.

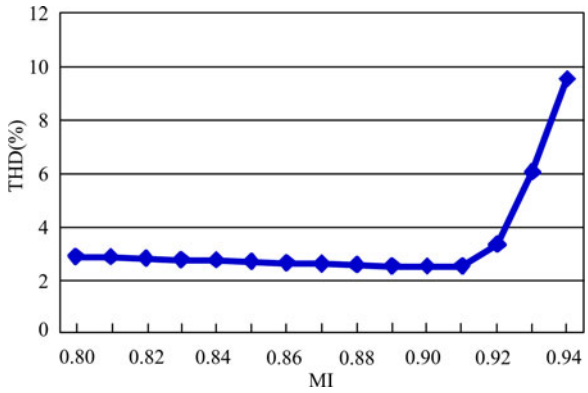

Fig. 17. THD versus MI.

The switching frequency f_s is 20 kHz. So the turn number of secondary side n_s is selected as 40, and the actual B_m is calculated to be 0.138 T.

F. Design Considerations of the Filter Inductor

The design of the filter inductor $L(L_a, L_b, L_c)$ should take both the ripple of harmonic current and current tracking performance into considerations [29]. The current variation of L_a in a switching cycle is

$$\begin{cases} \Delta i_1 = \dfrac{(S_b + S_c) n_p V_{\rm dc} T_1}{3 n_s L} & (S_a = 0) \\ \Delta i_2 = \dfrac{(-2 + S_b + S_c) n_p V_{\rm dc} T_2}{3 n_s L} & (S_a = 1) \end{cases}. \tag{34}$$

When $L_i (i = a, b, c)$ connects to the positive end of the transformer's voltage, S_i is 1. Otherwise, S_i is 0. To guarantee proper current tracking performance at the zero-crossing point of current, the upper limit of L should meet the following equations:

$$\frac{|\Delta i_1| - |\Delta i_2|}{T_s} \geq \frac{I_m \sin \omega T_s}{T_s} \approx I_m \omega \tag{35}$$

$$L \leq \frac{2 n_p V_{\rm dc}}{3 n_s I_m \omega} = \frac{2 n_p V_{\rm dc}}{3 n_s \dfrac{P}{3 \eta V_{aN}} \cdot \sqrt{2} \omega} = 0.169 \text{ H}. \tag{36}$$

To limit the current ripple of harmonic current at the peak point of current, the lower limit of L should meet the following equation:

$$|\Delta i_1| \approx |\Delta i_2| \leq \Delta i_{\max} \tag{37}$$

$$L \geq \frac{n_p V_{\rm dc} T_s}{6 n_s \Delta i_{\max}} = \frac{n_p V_{\rm dc} T_s}{6 n_s \cdot 20\% \cdot I_m} = 3.325 \text{ mH} \tag{38}$$

So the value of filter inductor is selected to be 3.3 mH.

VI. Simulation and Experimental Results

In order to verify the theoretical analysis, the proposed single-stage isolated three-phase bidirectional ac/dc converter is simulated by MATLAB/SIMULINK based on the control system in Fig. 3. Fig. 16 shows the harmonic analysis of A-phase current i_a under rectifier mode. It is clear that the converter achieves high power factor. Fig. 17 shows the relationship between the THD of output current and the modulation index (MI) by adjusting the transformer turns ratio. MI is defined as

$$\text{MI} = \frac{V_{ap}}{\frac{2}{\pi}\left(\frac{n_p}{n_s} V_{\rm dc}\right)}. \tag{39}$$

For the required peak value of phase-voltage V_{ap} and given input voltage $V_{\rm dc}$ under inverter mode, MI varies with the transformer's turn ratio. The current's THD increases a lot when MI exceeds 0.907. So the turn ratio should be chosen to make MI below 0.907, which is consistent with (32). However, the switches' voltage stress increases when MI decreases. So the design of the transformer's turn ratio should take both the current's THD and voltage stress into considerations. Although the current has minimum THD when MI is 0.907, appropriate margin should be set for the closed-loop regulation and MI is chosen to be 0.86.

A 3 kW prototype was built in the lab with the digital controller TMS320F2812. The components are as follows: Q_{i1-4}, $Q_{p1,2}$, Q_{s1-4}: IKW25N120T2; inductor magnetic core: KH250-060A; transformer magnetic core: EE85B; and driver: HCPL3120. The parameters and specifications are as follows:

1) AC line voltage: $v_{\rm ac} = 380\,\text{V}$;
2) AC voltage frequency: $f = 50\,\text{Hz}$;
3) DC voltage: $V_{\rm dc} = 380\,\text{V}$;
4) rated output power: $P_o = 3\,\text{kW}$;
5) filter inductor: $L = 3.3\,\text{mH}$;
6) filter capacitor: $C_o = 330\,\mu\text{F}^*4$;
7) transformer turns ratio: $n_p/n_s = 60/40$;
8) switching frequency: $f_s = 20\,\text{kHz}$.

Fig. 18 shows the experimental results under rectifier mode. Fig. 18(a) shows the driving signals of $Q_{a2,3}$, $Q_{b2,3}$, and $Q_{c2,3}$, and the zoomed-in area shows the switching sequence of sector 13, which is consistent with theoretical analysis. In rectifier mode, it is unnecessary to separate the driving waveforms of Q_{a2} and Q_{a3} according to the current direction of i_a for simplicity. They can also be separated for saving driving loss. Fig. 18(b) shows the waveforms of v_a, i_a, $v_{gs\_a2,3}$, and the voltage across the secondary winding v_{Tr_p}. Fig. 18(c) shows the waveforms of three-phase current.

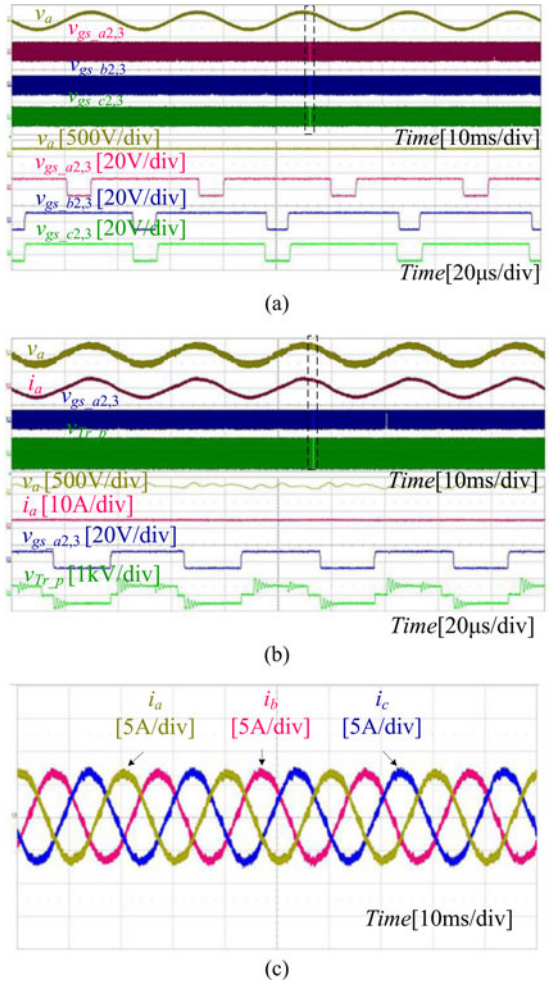

Fig. 18. Experimental results under rectifier mode.

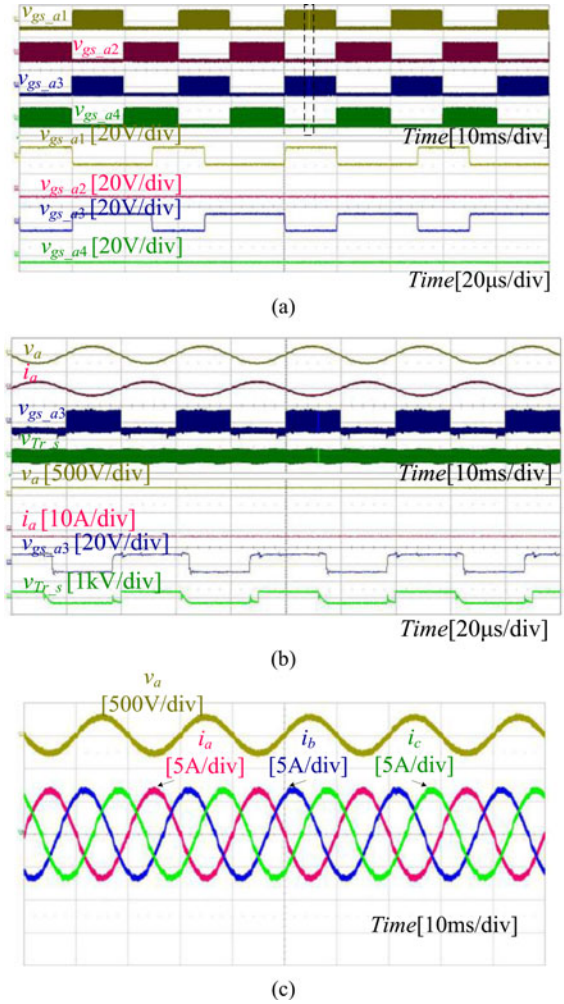

Fig. 19. Experimental results under inverter mode.

Fig. 19 shows the experimental results under inverter mode. Fig. 19(a) shows the driving signals of Q_{a1-4}. It shows that no dead time is needed between v_{gs_a1} and v_{gs_a3} to avoid the shoot-through problem by the proposed control strategy. Fig. 19(b) shows the waveforms of v_a, i_a, v_{gs_a3}, and the voltage across the secondary winding v_{Tr_s}. The zoomed-in area shows the operating waveforms of sector 13. It is seen that the transformer achieves the voltage–second balance. Fig. 19(c) shows the waveforms of v_a and three-phase current. The current's THD is tested to be 1.914%. Fig. 20 shows the efficiency curves of theoretical analysis and experimental result. It is concluded that the proposed SVPWM algorithm achieves the voltage–second balance of the transformer and the experimental results verified the theoretical analysis well.

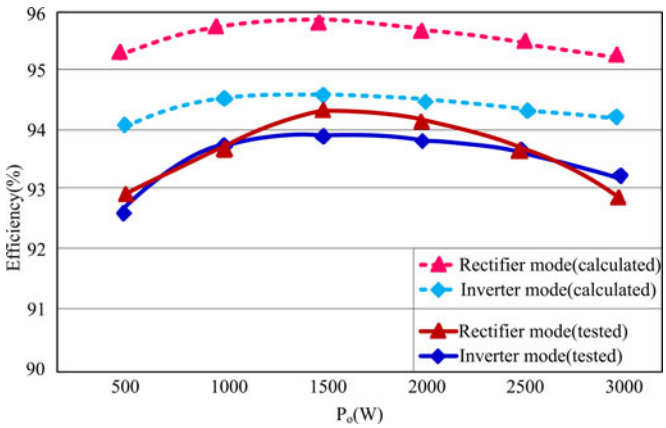

Fig. 20. Efficiency curve.

VII. Conclusion

This paper proposes a three-phase isolated bidirectional ac/dc converter and its SVPWM algorithm. It achieves sinusoidal ac current, buck–boost ac/dc conversion, and high-frequency isolation with single-stage structure. Compared with the traditional two-stage converter, it removes the bulk decoupling capacitors and filter inductor of dc side and has higher power density. The converter does not have any shoot-through problem without extra dead time. A 3 kW prototype was built in the lab and the experimental results verify the theoretical analysis well.

REFERENCES

[1] M. R. Islam, Y. Guo, and J. Zhu, "A high-frequency link multilevel cascaded medium-voltage converter for direct grid integration of renewable energy systems," *IEEE Trans. Power Electron.*, vol. 29, no. 8, pp. 4167–4182, Aug. 2014.

[2] H. Valderrama-Blavi, J. M. Bosque, F. Guinjoan, L. Marroyo, and L. Martínez-Salamero, "Power adaptor device for domestic dc microgrids based on commercial MPPT inverter," *IEEE Trans. Ind. Electron.*, vol. 60, no. 3, pp. 1191–1203, Mar. 2013.

[3] X. Lu, K. Sun, J. M. Guerrero, J. C. Vasquez, and L. Huang, "State-of-charge balance using adaptive droop control for distributed energy storage systems in DC microgrid applications," *IEEE Trans. Ind. Electron.*, vol. 61, no. 6, pp. 2804–2815, Jun. 2014.

[4] A. Fukui, T. Takeda, K. Hirose, and M. Yamasaki, "HVDC power distribution systems for telecom sites and data centers," in *Proc. Power Electron. Conf.*, Sapporo, 2010, pp. 874–880.

[5] A. Sanino, G. Postiglione, M. H. J. Bollen, "Feasibility of a DC network for commercial facilities," *IEEE Trans. Ind. Appl.*, vol. 39, no. 5, pp. 1499–1507, Sep. 2003.

[6] A. Matsumoto, A. Fukui, T. Takeda, K. Hirose, and M. Yamasaki, "Development of 400 Vdc power distribution system and 400 Vdc output rectifier," in *Proc. IEEE 31st Int. Telecommun. Energy Conf.*, Incheon, 2009, pp. 1–5.

[7] T.-F. Wu, C.-H. Chang, L.-C Lin, and Y.-C. Chang, "DC-bus voltage control for three-phase bi-directional inverter in DC microgrid applications," in *Proc. IEEE Appl. Power Electron. Conf. Expo.*, Orlando, FL, USA, 2012, pp. 377–383.

[8] A. Stupar, T. Friedli, J. Minibock, and J. W. Kolar, "Towards a 99% efficient three-phase buck-type PFC rectifier for 400V DC distribution systems," *IEEE Trans. Power Electron.*, vol. 27, no. 4, pp. 1732–1744, Apr. 2012.

[9] S. Dasgupta, S. N. Mohan, S. K. Sahoo, and S. K. Panda, "Application of four-switch-based three-phase grid-connected inverter to connect renewable energy source to a generalized unbalanced microgrid system," *IEEE Trans. Ind. Electron.*, vol. 60, no. 3, pp. 1204–1215, Mar. 2013.

[10] W. Li, X. Ruan, C. Bao, D. Pan, and X. Wang, "Grid synchronization systems of three-phase grid-connected power converters: A complex-vector-filter perspective," *IEEE Trans. Ind. Electron.*, vol. 61, no. 4, pp. 1855–1870, Apr. 2014.

[11] P. Rodríguez, A. Luna, R. Muñoz-Aguilar, I. Etxeberria-Otadui, R. Teodorescu, and F. Blaabjerg, "A stationary reference frame grid synchronization system for three-phase grid-connected power converters under adverse grid conditions," *IEEE Trans. Power Electron.*, vol. 27, no. 1, pp. 99–112, Jan. 2012.

[12] Z. Yin, J. Liu, and Y. Zhong, "Study and control of three-phase PWM rectifier based on dual single-input single-output model," *IEEE Trans. Ind. Informat.*, vol. 9, no. 2, pp. 1064–1073, May 2013.

[13] B. Yin, R. Oruganti, S. Kumar, and A. Bhat, "A simple single-input single-output (SISO) model for three-phase PWM rectifiers," *IEEE Trans. Power Electron.*, vol. 24, no. 3, pp. 620–631, Mar. 2009.

[14] Y. Yang, P. C. Loh, P. Wang, and F. H. Choo, "One-cycle-controlled three-phase PWM rectifiers with improved regulation under unbalanced and distorted input-voltage conditions," *IEEE Trans. Power Electron.*, vol. 25, no. 11, pp. 2786–2796, Nov. 2010.

[15] L. Chen, A. Amirahmadi, Q. Zhang, N. Kutkut, and I. Batarseh , "Design and implementation of three-phase two-stage grid-connected module integrated converter," *IEEE Trans. Power Electron.*, vol. 29, no. 8, pp. 3881–3892, Aug. 2014.

[16] B. Guo, F. Xu, Z. Zhang, Z. Xu, F. Wang, L. M. Tolbert, and J. B. Blalock , "Compensation of input current distortion in three-phase buck rectifiers," in *Proc. IEEE Appl. Power Electron. Conf. Expo.*, Long Beach, CA, USA, 2013, pp. 930–938.

[17] J. W. Kolar, U. Drofenik, and Franz C. Zach, "VIENNA rectifier II—A novel single-stage high-frequency isolated three-phase PWM rectifier system," *IEEE Trans. Ind. Electron.*, vol. 46, no. 4, pp. 674–691, Aug. 1999.

[18] V. Vlatkovic, D. Borojevic, and F. C. Lee, "A zero-voltage switched, three-phase isolated PWM buck rectifier," *IEEE Trans. Power Electron.*, vol. 10, no. 2, pp. 148–157, Mar. 1995.

[19] D. S. Greff, R. Da Silva, S. A. Mussa, A. Perin, and I. Barbi, "A three-phase buck rectifier with high-frequency isolation by single-stage," in *Proc. IEEE Power Electron. Spec. Conf.*, 2008, pp. 1129–1133.

[20] P. Knaup, "Inverter," International Patent WO/2007/048 420, May 3, 2007.

[21] G. Carrasco and C. A. Silva, "Space vector PWM method for five-phase two-level VSI with minimum harmonic injection in the overmodulation region," *IEEE Trans. Ind. Electron.*, vol. 60, no. 5, pp. 2042–2053, May 2013.

[22] S. Pan, J. Pan, and Z. Tian, "A shifted SVPWM method to control DC-link resonant inverters and its FPGA realization," *IEEE Trans. Ind. Electron.*, vol. 59, no. 9, pp. 3383–3391, Sep. 2012.

[23] G. Tan, Q. Deng, and Z. Liu, "An optimized SVPWM strategy for five-level active NPC (5L-ANPC) converter," *IEEE Trans. Power Electron.*, vol. 29, no. 1, pp. 386–395, Jan. 2014.

[24] S. Manias, A. R. Prasad, and P. D. Ziogas, "A 3-phase inductor fed SMR converter with high frequency isolation, high power density and improved power factor," in *Proc. IEEE 22nd Ind. Appl. Soc. Annu. Meet. Conf. Rec.*, 1987, pp. 253–263.

[25] F. Z. Peng, "Z-source inverter," *IEEE Trans. Ind. Appl.*, vol. 39, no. 2, pp. 504–510, Mar. 2003.

[26] S. Jiang, D. Cao, and F. Z. Peng, "High frequency transformer isolated Z-source inverters," in *Proc. IEEE Appl. Power Electron. Conf.*, Fort Worth, TX, USA, 2011, pp. 442–449.

[27] C. Qiao and K. Smedley, "Three-phase unity power factor star connected switch (Vienna) rectifier with unified constant frequency integration control," *IEEE Trans. Power Electron.*, vol. 18, no. 4, pp. 952–957, Jul. 2003.

[28] J. A. Sabate, V. Vlatkovic, R. B. Ridley, F. C. Lee, and B. H. Cho, "Design considerations for high-voltage high-power full-bridge zero-voltage-switching PWM converter," in *Proc. Appl. Power Electron. Conf.*, Mar. 1990, pp. 275–284.

[29] X. Zhang. *Study on the PWM Rectifier and its Control Strategies*, Hefei University of Technology, Hefei, China, 2003.

Ling Gu (S'13) was born in Wuxi, Jiangsu Province, China, in 1988. She received the B.S. degree in electrical engineering from the Nanjing University of Aeronautics and Astronautics, Nanjing, China, in 2011, where she is currently working toward the Ph.D. degree.

Her current research interests include low-voltage high-current conversion techniques and renewable power systems.

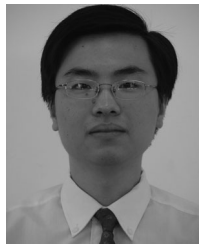

Ke Jin (S'04–M'09) was born in Nanjing, China, in 1978. He received the B.S., M.S., and Ph.D. degrees in electrical engineering from the Nanjing University of Aeronautics and Astronautics (NUAA), Nanjing, in 2000, 2003, and 2006, respectively.

From 2007 to 2008, he was a Postdoctoral Researcher with the Center for Power Electronics Systems, Virginia Polytechnic Institute and State University, Blacksburg, VA, USA. He is currently a Professor with the College of Automation Engineering, NUAA. He has authored more than 40 technical papers published in international journals and conference proceedings. He holds eight Chinese patents and one U.S. patent. Eight Chinese patents are pending. His main research interests include high-frequency soft-switching conversion, low-voltage high-current conversion techniques, and renewable power systems.